

Studying the ωN elastic and inelastic cross section with nucleons^{*}

Ye.S. Golubeva¹, W.Cassing², L.A. Kondratyuk³, A. Sibirtsev² and M. Büscher⁴

¹ Institute for Nuclear Research, 60th October Anniversary Prospect 7A,
117312 Moscow, Russia

² Institut für Theoretische Physik, Universität Giessen,
D-35392 Giessen, Germany

³ Institute of Theoretical and Experimental Physics, B. Chermushkinskaya 25,
117259 Moscow, Russia

⁴ Forschungszentrum Jülich, Institut für Kernphysik, D-52425 Jülich, Germany

Received: date / Revised version: date

Abstract. We explore the possibility to measure the elastic and inelastic ωN cross section in $p+d \rightarrow d+\omega+p_{sp}$ and $p+A$ reactions. Our studies indicate that the elastic scattering cross sections can be determined for ω momenta above 1 GeV/c in $p+d$ reactions by gating on high proton spectator momenta whereas the ωN absorption cross section down to low relative ω momenta is most effectively studied in $p+A$ reactions at beam energies 2.0–2.7 GeV.

PACS. 13.75.Cs Nucleon-nucleon interactions – 25.40.-h Nucleon-induced reactions – 25.10.+s Nuclear reactions involving few-nucleon systems – 11.80.Fv Eikonal approximation – 24.10.Lx Monte Carlo simulations

1 Introduction

The ω -meson properties at finite nuclear density have become of recent interest especially in the context of dilepton studies [1, 2], where one hopes to see a shift of the meson pole e.g. at density $\rho_0 \approx 0.16 \text{ fm}^{-3}$ [3, 4, 5, 6]. However, the in-medium properties of the vector mesons - as reflected in their spectral functions - are presently a matter of strong debate. Whereas at high baryon density and/or temperature some scaling of the meson poles with the scalar quark condensate $\langle \bar{q}q \rangle$ might be adequate [7], the properties of the mesons in a hadron gas at low density are essentially determined by the scattering amplitudes with the hadrons in the local environment [8]. By means of dispersion relations the real and imaginary part of these scattering amplitudes – in the low density approximation – directly convert to mean-field potentials and scattering rates, respectively [9]. Thus it is of profound interest to obtain more precise information especially about the ωN cross sections to construct its spectral function at low baryon density.

We recall that the strong coupling of the ρ -meson to nucleon resonances leads to large inelastic cross sections with nucleons at low relative momenta which in turn results in a large collisional width at density ρ_0 [8, 9, 10, 11, 12, 13]. If this *melting* of the ρ -meson will also occur for the ω meson is of major importance for dilepton experiments, that aim at detecting moderate but clear peaks in the dilepton invariant mass spectra. Though there are a couple of theoretical estimates for the ωN cross sections [10, 11, 12, 14, 15, 16] the theoretical predictions

widely differ such that related experiments will have to clarify the situation.

Moreover, the amplitude for ω -meson production in proton-nucleon reactions close to threshold so far is scarcely known – especially with a deuteron in the final state – and of interest in itself.

In this work we aim at contributing to the latter question by investigating theoretically within the Multiple Scattering Monte Carlo (MSMC) approach and transport model calculations, to what extent we might obtain experimental information from various reactions at existing accelerators that can be performed in the near future. In Section 2 we will study in detail the perspectives of the reaction $p + d \rightarrow d + \omega + p_{sp}$ close to threshold. In Section 3 proton induced reactions on nuclei will be investigated within a coupled channel transport approach to explore the production and propagation of the ω -meson in finite nuclei whereas Section 4 is devoted to a summary of our work.

2 Effects from ω rescattering in the reaction

$p+d \rightarrow d+\omega+p_{sp}$

In Ref. [17] we have considered the cross section of the reaction $p+d \rightarrow d+\omega+p$ within the framework of the spectator mechanism close to threshold energies (see diagram a) in Fig. 1). This mechanism gives the dominant contribution to the cross section if the momentum of the proton-spectator from the deuteron is below 100–150 MeV/c. The amplitude corresponding to the diagram a) of Fig. 1 can be written in the following form in the

^{*} supported by DFG, RFFI and Forschungszentrum Jülich.

deuteron rest frame

$$M_a = f(pn \rightarrow dV) \int d^3\mathbf{r} \exp(-i\mathbf{p}_2\mathbf{r}) \phi_d(\mathbf{r}), \quad (1)$$

where V is the vector meson (ω), \mathbf{p}_2 is the proton spectator momentum, $\phi_d(\mathbf{r})$ is the deuteron wave function and $f(pn \rightarrow dV)$ is the amplitude of the reaction $pn \rightarrow dV$, related to the differential lab. cross section as

$$\frac{d\sigma(pn \rightarrow dV)}{d\Omega} = |f(pn \rightarrow dV)|^2. \quad (2)$$

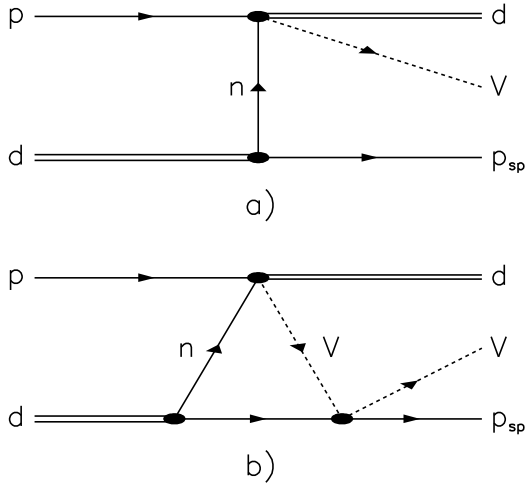


Fig. 1. The diagrams for vector meson (V) production in the $p+d \rightarrow d+V+p_{sp}$ reaction without (a) and with VN rescattering (b).

The produced vector meson can rescatter elastically on the proton-spectator, thus transferring momenta larger than 200 MeV/c. Near threshold the momentum of the produced ω meson is quite large: about 0.8-1 GeV/c. Therefore its wave length is much smaller than the average distance between two nucleons in a deuteron. In this case we can describe the rescattering amplitude (see diagram b) in Fig. 1) within the framework of the eikonal approximation (cf. Ref. [18])

$$M_b = -f(pn \rightarrow dV) \int d^3\mathbf{r} \exp(-i\mathbf{p}_2\mathbf{r}) \Theta(z) \Gamma(\mathbf{b}) \phi_d(\mathbf{r}), \quad (3)$$

where the z -axis is directed along the V -meson momentum. The elastic Vp -scattering amplitude is related to the profile function $\Gamma(\mathbf{b})$ by the standard expression

$$f(Vp \rightarrow Vp) = \frac{1}{2\pi ik} \int d^2\mathbf{b} \exp(-i\mathbf{q}\mathbf{b}) \Gamma(\mathbf{b}) \quad (4)$$

with k denoting the lab. momentum of the V -meson and \mathbf{q} the momentum transfer.

The probability to detect the deuteron at the solid angle $d\Omega_d$ in coincidence with the spectator of momentum \mathbf{p}_2 is related to the differential cross section as

$$\frac{d^5\sigma(pd \rightarrow dVp_2)}{d\Omega d^3p_2} = |M_a + M_b|^2. \quad (5)$$

The probability for the produced meson to rescatter can be found by integrating the term proportional to $|M_b|^2$, which is equal to

$$W = \sigma_{el}(Vp \rightarrow Vp) \int dz \Theta(z) |\phi_d(\mathbf{b} = 0, z)|^2. \quad (6)$$

Now the momentum distribution of the spectators can be written in the form

$$\frac{dN(p)}{p^2 dp} = N(|\psi_d(p)|^2 + |\Psi_{resc}(p)|^2 + \text{Interference Term}), \quad (7)$$

where the first term is the contribution of the spectator mechanism, with $\psi_d(p)$ denoting the deuteron wave function in momentum space, while N is the normalization factor. The second term $|\Psi_{resc}(p)|^2$ appears due to the rescattering of all particles in the final state on the proton-spectator added incoherently with the probabilities defined by Eq. (6). The interference between the spectator and rescattering amplitudes is only important in a narrow region of spectator momenta, where both contributions are of the same order of magnitude. For a more detailed discussion of this point see, e.g. Refs. [18, 19, 20, 21]).

In order to obtain closer information on the vector meson rescattering we employ the Multiple Scattering Monte Carlo (MSMC) approach. An earlier version of this approach, denoted as Intra-Nuclear Cascade (INC) model, has been applied to the analysis of η and ω production in $\bar{p}A$ and pA interactions in Refs. [22, 23], respectively. Recently this version of the INC model has been extended to incorporate in-medium modifications of the mesons produced [4, 5] in hadron-nuclear collisions. For an explicit presentation of the production cross sections employed we refer the reader to Ref. [5] or the review [1].

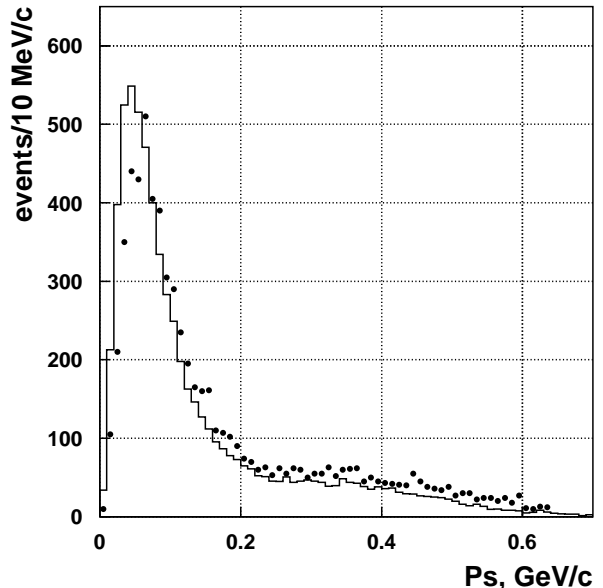


Fig. 2. Momentum distribution of proton-spectators in the reaction $\bar{p}d \rightarrow 3\pi^+ 2\pi^- p$. The data are taken from Ref. [25] while the solid line is calculated using Eq. (7).

However, the INC model is valid only for medium and heavy nuclei and cannot be directly applied to deuterons. In order to perform simulations of scattering events in the case of hadron – deuteron interactions we use the Monte Carlo approach for the description of single and double scattering terms. The momentum distribution of a nucleon in the deuteron is described by the Fourier transformed deuteron wave function squared $|\psi_d(p)|^2$. The total probability of rescattering is calculated for each secondary particle using Eq.(6). All events are generated using realistic angular distributions for the elementary subprocesses. In the case of ω meson rescattering this information is not available from data and we employ different assumptions on its cross section, i.e. in magnitude and angular distribution.

Experimentally, proton-spectator spectra have been measured in $\bar{p}d$ annihilation [24,25] to some extent. As an example – and to testify the applicability of the model to such type of reactions – we present in Fig. 2 the calculated momentum distribution of proton spectators in the reaction $\bar{p}d \rightarrow 3\pi^+ 2\pi^- p$ at rest in comparison to the data from Ref. [25]. These data are easy to interpret: the sharp peak with a maximum near 60 MeV/c corresponds to the spectator mechanism and the long tail above 300 MeV/c is due to the rescattering of pions. The solid line in Fig. 2 is calculated using Eq. (7) (without the interference term), where the deuteron wave function was taken in the parameterization of Ref. [26] with S- and D-waves included. The dependence of the second term on the momentum p in the lab. system is determined by the kinematical conditions (like the mass of the rescattered particle) and by the angular dependence of the pion-nucleon scattering amplitude. We find that the spectrum calculated by the MSMC approach is in good agreement with the experimental data.

The same approach was used to simulate the momentum distributions of spectator protons in the reaction $p+d \rightarrow d+\omega+p_{sp}$. Since the elastic rescattering cross section of the ω -meson is basically unknown and especially its angular distribution at high relative momenta, we study the observable effects within different models. In Fig. 3 we present three assumptions for the angular distribution of ωN elastic rescattering (upper left). These assumptions correspond to a parameterization of the differential cross section $d\sigma/dt = C \exp(bt)$ with slope parameters $b = 0, 6$ and 12 GeV^{-2} , respectively.

The resulting spectator momentum distributions are shown in the upper right part of Fig. 3. The lowest (dotted) histogram describes the contribution of the spectator term when rescattering is absent. In this case the proton momentum spectrum only extends to 450 MeV/c. The most pronounced effect from rescatterings is seen for the isotropic model (solid histogram) where the proton momentum spectrum extends to 1 GeV/c.

Furthermore, the distributions in the azimuthal angle Φ between the scattering planes $p-p_\omega$ and $p-p_{sp}$ for spectators with $p_{sp} \leq 150 \text{ MeV/c}$ (middle left), $150 \leq p_{sp} \leq 300 \text{ MeV/c}$ (middle right), $300 \leq p_{sp} \leq 450 \text{ MeV/c}$ (lower left) and for fast spectators with $p_{sp} \geq 450 \text{ MeV/c}$ (lower right), show the most pronounced rescattering effects for fast spectators in line with the upper right part of the figure.

It is clearly seen that the spectator mechanism dominates at $p_{sp} \leq 300 \text{ MeV/c}$ while at $p_{sp} \geq 450 \text{ MeV/c}$ the main contribution stems from the rescattering term. The best way to select the rescattering term is to look for the correlation be-

tween the azimuthal angles of the two scattering planes $p-p_\omega$ and $p-p_{sp}$ (lower figures). This correlation is much more pronounced for fast spectators ($p_{sp} \geq 450 \text{ MeV/c}$) than for slower ones ($p_{sp} \leq 300 \text{ MeV/c}$). It is worth to point out that the slope of the spectator spectrum depends on the slope of the $\omega-p$ angular distribution, while the correlation in the angle Φ depends mainly on the value of the ωN elastic cross section.

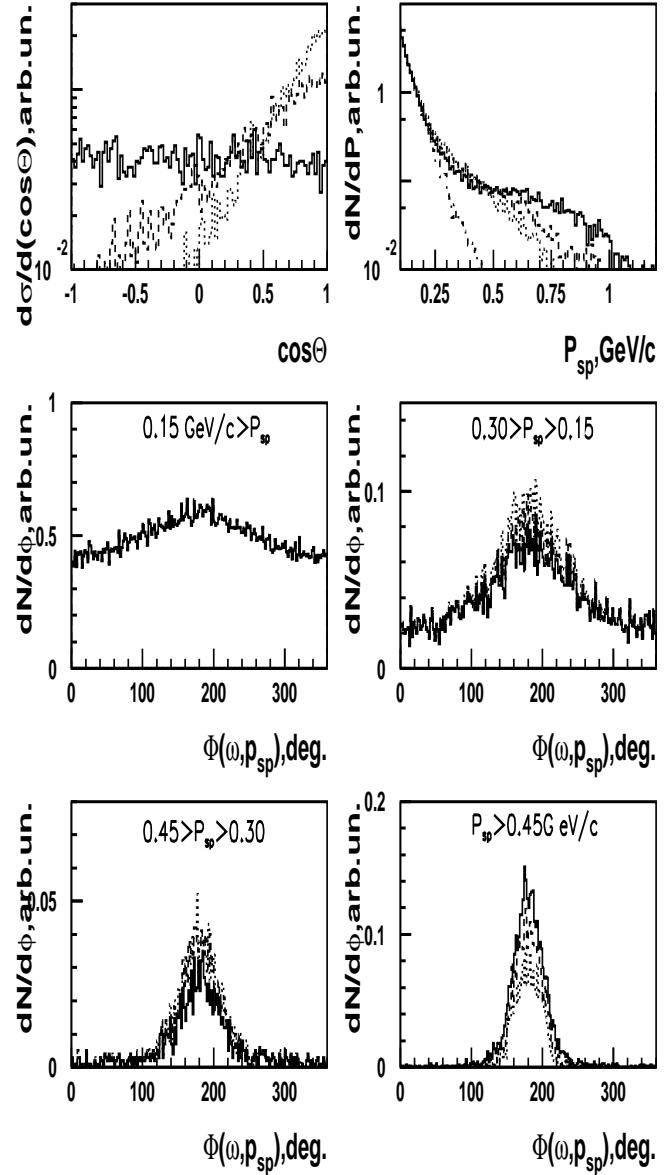


Fig. 3. Angular distribution of ωN elastic rescattering (upper left) within 3 different models indicated by the solid, dashed and dotted histograms (see text). The resulting proton-spectator momentum distributions are shown in the upper right part for the 3 models in the reaction $p+d \rightarrow d+\omega+p_{sp}$. In all calculations the ωN rescattering cross section $\sigma_{el}=40 \text{ mb}$ was assumed. The distributions in the azimuthal angle Φ between the scattering planes $p-p_\omega$ and $p-p_{sp}$ for spectators with $p_{sp} \leq 150 \text{ MeV/c}$ (middle left), $150 \leq p_{sp} \leq 300 \text{ MeV/c}$ (middle right), $300 \leq p_{sp} \leq 450$ (lower left) and for fast spectators with $p_{sp} \geq 450 \text{ MeV/c}$ (lower right) are shown additionally.

Thus performing a cut for $p_{sp} \geq 250$ MeV/c and $150^\circ < \Phi(\omega, p_{sp}) < 210^\circ$ one can determine essentially the overall magnitude of the ωN elastic cross section (cf. upper part of Fig. 4), whereas the number of events as a function of the cut in the proton-spectator momentum p_{sp} provides information on the ω - N angular distribution. This is demonstrated in the lower part of Fig. 4 for the 3 models of the ω - p angular distributions, where the solid, dashed and dotted lines correspond to the upper left part of Fig. 3.

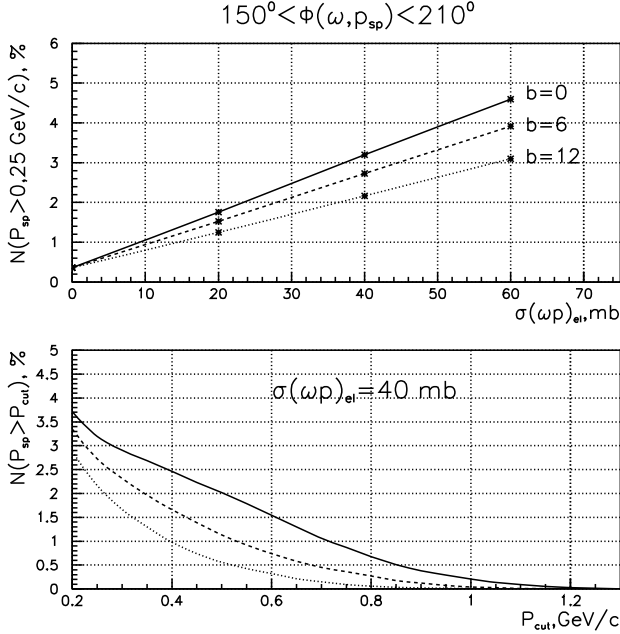


Fig. 4. The number of events for the cut $p_{sp} \geq 250$ MeV/c and $150^\circ < \Phi(\omega, p_{sp}) < 210^\circ$ as a function of the elastic ωp cross section for 3 different angular distributions (solid, dashed and dotted lines) from the upper left part of Fig. 3 is displayed in the upper part of the figure. The lower part shows the number of events as a function of the cut in the proton-spectator momentum p_{sp} for the 3 different angular distributions assuming an overall magnitude of $\sigma_{el}(\omega p) = 40$ mb in the reaction $p+d \rightarrow d+\omega+p_{sp}$. The corresponding slope parameters b are given in GeV^{-2} (see text).

It is worth to point out that the relative contribution of the rescattering term is about a few percent as compared to the spectator term. In the case of small spectator momenta, when the spectator term is dominant, the reaction $p+d \rightarrow d+\omega+p_{sp}$ can be identified by the missing mass method measuring the forward deuteron in coincidence with a slow spectator proton. We note that the spectator detection with thin semiconductor counters has already successfully been applied for η -meson production in pd collisions at CELSIUS [27, 28]. However, the selection of the reaction $p+d \rightarrow d+\omega+p_{sp}$ with fast ($p_{sp} \geq 250$ MeV/c) rescattered spectator protons is more difficult since background particles (e.g. π -mesons) can be misidentified as spectator protons. Thus, the direct detection of the produced ω -mesons by the detection of its decay products like $\pi^0 \gamma$ is mandatory. We suggest to use a neutral particle detector and to gate on three energetic photons, where two photons should be

correlated in their invariant mass to the π^0 whereas the third photon should add to the invariant mass of the ω -meson according to its Dalitz decay $\omega \rightarrow \pi^0 + \gamma$ with a branching ratio of $\simeq 8.5\%$.

The momentum and angular distributions of π^0 -mesons and photons in the reaction $p+d \rightarrow d+\omega(\rightarrow \pi^0 \gamma)+p_{sp}$ at $T_p=2$ GeV are shown in Fig. 5. The momentum spectra of pions and photons have maxima at 0.5 GeV/c. Thus the detection of such energetic photons will be a very good trigger for ω production, i.e. the selection of the reaction can be done by measuring the ω with a fast forward deuteron in coincidence. We note that such measurements might well be performed at COSY-Jülich.

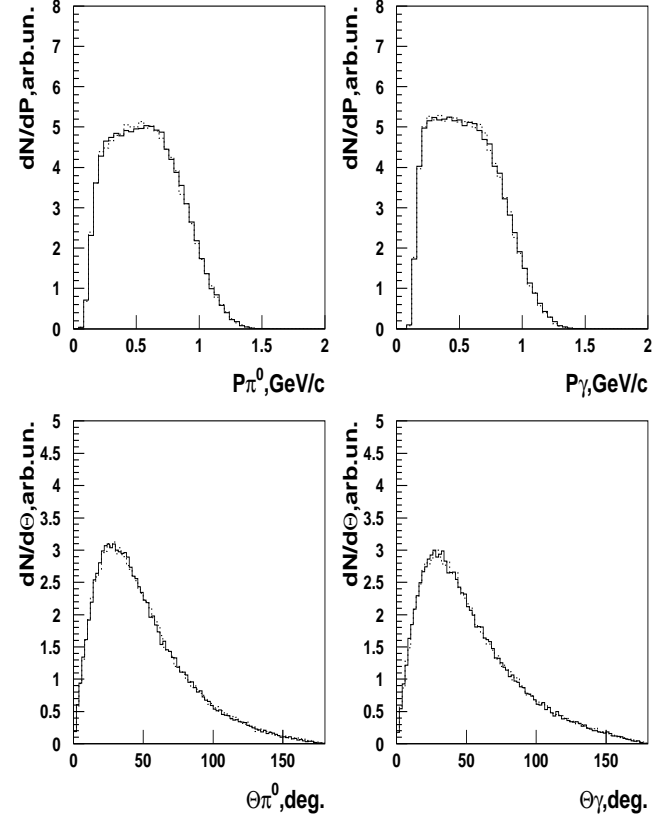


Fig. 5. The momentum and angular distributions of π^0 mesons and photons from the reaction $p+d \rightarrow d+\omega(\rightarrow \pi^0 \gamma)+p_{sp}$ at $T_p=2$ GeV.

3 Proton induced reactions on nuclei

The production of vector mesons in proton induced reactions on light and heavy nuclei has been studied before for ρ -meson propagation in the medium by looking at $\pi^+ \pi^-$ invariant mass spectra in Ref. [29]. For the dynamical studies we again employ the coupled channel transport model [30] with elementary production cross sections as described in Refs. [1]. The transport approach [30] allows to account for the final state interactions (FSI) of all hadrons and especially the elastic and inelastic ωN scatterings. For the experimental detection of the ω -meson we again suggest to gate on three energetic photons.

In order to include the effects from ωN elastic rescattering we employ the cross section from Ref. [16] in the parameterization

$$\sigma_{el} = 5.4 + 10 * \exp(-0.6p_\omega) \text{ [mb]}, \quad (8)$$

where p_ω is the ωN relative laboratory momentum in GeV/c. For the inelastic channels we have to consider various reactions (cf. Ref. [16]). Among them the $\omega + N \rightarrow \pi + N$ cross section can be determined quite well from the available data on the exclusive ω production in πN reactions from Ref. [31] by exploiting detailed balance. The ωN inelastic cross sections due to other reaction channels have been calculated in Ref. [16] by a meson-exchange model and, in principle, are determined within the uncertainties of the coupling constants and the form factors employed. As a guide we thus use the inelastic ωN cross section σ_{inel} from Ref. [16] within the parameterization

$$\sigma_{inel} = 20 + 4.0/p_\omega \text{ [mb]}, \quad (9)$$

with p_ω given in GeV/c.

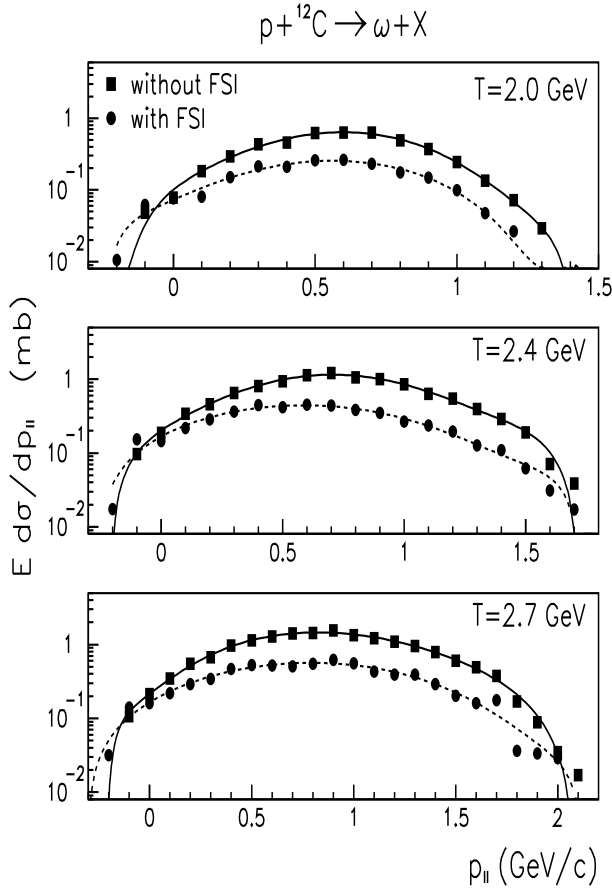


Fig. 6. The longitudinal momentum distribution of ω -mesons produced in $p+^{12}\text{C}$ collisions at 2.0, 2.4 and 2.7 GeV. The symbols show the transport calculations while the lines are drawn to guide the eye. The squares show the calculations without ωN final state interactions while the full dots include FSI.

The momentum distribution of ω -mesons in beam direction,

$$E \frac{d\sigma}{dp_{||}} = \int dp_{\perp}^2 E \frac{d^3\sigma}{d^3p}, \quad (10)$$

is shown in Fig. 6 for $p+^{12}\text{C}$ collisions at beam energies of 2.0, 2.4 and 2.7 GeV. The dashed lines in Fig. 6 (full dots) show the calculations by taking into account the elastic and inelastic ωN interactions, while the solid lines indicate the results obtained without FSI (full squares).

At all energies considered the ω longitudinal momentum distribution in the laboratory is extending over a broad momentum regime from negative momenta even up to $p_{||} \approx 2.0$ GeV/c at $T_{lab}=2.7$ GeV. By comparing the dashed and solid lines we find a substantial reduction of the ω -meson yield at medium and high momenta even for ^{12}C . Furthermore, for ω momenta in the Fermi-momentum regime $p_F \leq 0.23$ GeV/c a suppression is less obvious. This is due to elastic $\omega N \rightarrow \omega N$ scattering which essentially populates low $p_{||}$ in the laboratory system.

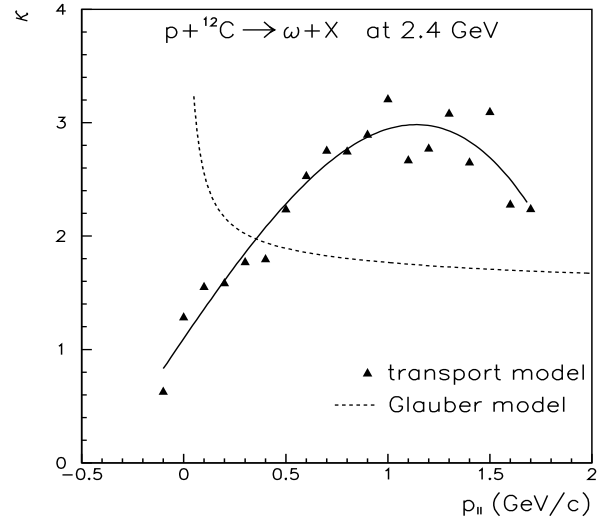


Fig. 7. The ratio κ of the ω -meson spectrum without FSI to the ω -spectrum including FSI (triangles) from the transport calculation for $p+^{12}\text{C}$ collisions at 2.4 GeV. The solid line is drawn to guide the eye while the dotted line shows a Glauber calculation including the momentum dependent ωN cross section.

The latter phenomenon is more clearly demonstrated in Fig. 7 where we display the ratio κ of the ω spectrum without FSI to the ω spectrum including FSI (triangles) from the transport calculation for $p+^{12}\text{C}$ at 2.4 GeV. The solid line in Fig. 7 is drawn to guide the eye. Moreover, since the Glauber approximation is traditionally considered [32,33,34,35] as an effective way to evaluate the cross section of an unstable particle with nucleons we perform a comparison between the Glauber model and the results from the transport approach.

We recall that within the Glauber model the A-dependence for ω -meson production and propagation in the nucleus is given

as [36]

$$A_{eff} = \int_0^{+\infty} b db \int_{-\infty}^{+\infty} \rho(b, z) dz \int_0^{2\pi} d\phi \times [\exp(-\sigma_{pN} \int_{-\infty}^z \rho(b, \xi) d\xi - \sigma_{\omega N} \oint \rho(\mathbf{r}_\zeta) d\zeta)], \quad (11)$$

where $\rho(r)$ is the single-particle density distribution normalized to the target mass number. The last integration in Eq. (11) proceeds over the path of the produced ω -meson

$$r_\zeta^2 = (b + \zeta \cos\phi \sin\theta)^2 + (\zeta \sin\phi \sin\theta)^2 + (z + \zeta \cos\theta)^2, \quad (12)$$

where θ is the emission angle of the ω -meson relative to the beam direction. Moreover, σ_{pN} is the pN cross section while $\sigma_{\omega N}$ is the total ωN cross section.

Within the Glauber model the $p_{||}$ -dependence of the factor κ is given by the ratio of A_{eff} – calculated with the momentum dependent ωN cross section (9) – to the result for $\sigma_{\omega N}=0$. The dashed line in Fig. 7 shows the factor κ calculated by Eq. (11). It is clear that the calculations by the Glauber model fail in describing the FSI as generated by the transport calculation since the Glauber analysis discards elastic rescattering and accordingly misses the population of the low momentum part of the ω spectrum. Thus the factor κ calculated by the transport model substantially differs from the Glauber calculations at low ω -meson momenta. Furthermore the difference at $p_{||} > 500$ MeV/c is due to the fact that the transport calculations account for the ω production by secondary production processes, while the calculations by the Glauber model do not.

Indeed, we note that at subthreshold energies in $p+A$ reactions the secondary production channel with an intermediate pion ($p+N \rightarrow N+N+\pi$, $\pi+N \rightarrow \omega+N$) is the dominant one according to the studies performed in Refs. [36,37]. On the other hand, the calculations by Eq. (11) account only for the direct $pN \rightarrow pN\omega$ production mechanism. Thus the application of the Glauber model is not appropriate in this case for an experimental analysis.

The mass dependence of the total production cross section of mesons can be exploited to provide some information on the strength of the meson absorption cross section. In this respect we show in Fig. 8 (full dots) the expected mass A -dependence of ω mesons from $p+A$ reactions at beam energies $T_p=2.0, 2.4$, and 2.7 GeV as calculated by the transport model without including FSI. The cross sections can be well described at fixed energy by a power law

$$\sigma(p+A \rightarrow \omega+X) \sim A^\alpha, \quad (13)$$

where the parameter α sheds some light on the reaction mechanism. The solid lines in Fig. 8 show a fit to the transport model calculations with parameters α indicated in the figure. Furthermore, for the direct $p+N \rightarrow \omega+p+N$ production (neglecting the ω -meson FSI) we expect $\alpha \approx 0.75$ from the Glauber model (dashed lines in Fig. 8) which, however, underestimates the mass dependence obtained from the transport model calculations at all energies and especially at $T_p=2$ GeV.

As discussed in Ref. [36]-[39] the higher power in A is due to secondary reaction channels involving an intermediate

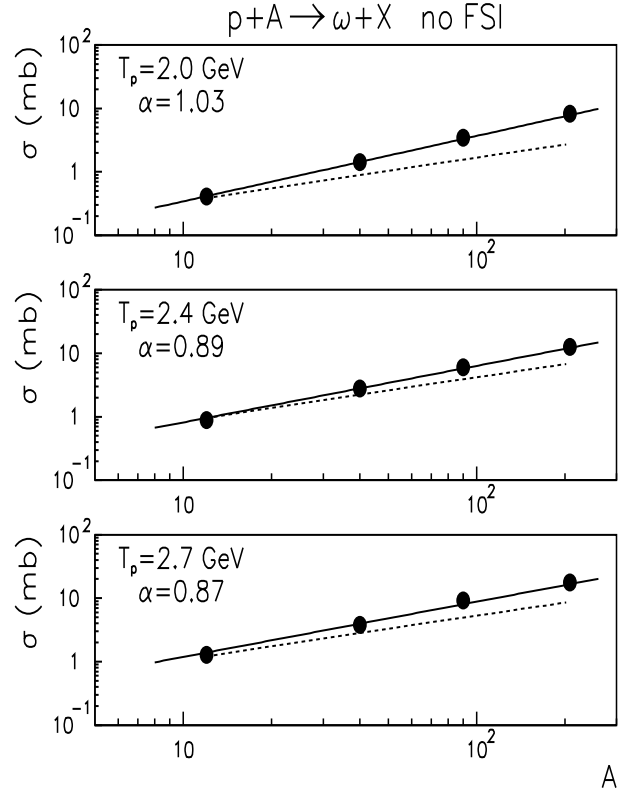


Fig. 8. The A -dependence of ω -meson production from $p+A$ reactions at beam energy $T_p=2.0, 2.4$, and 2.7 GeV calculated without FSI. The full dots show the transport model results while the solid lines are a fit by Eq. (13) with parameters α as indicated in the figures. The dashed lines show the calculations by the Glauber model without FSI, which provide $\alpha \approx 0.75$.

pion, which are more frequent in heavy nuclear targets and at lower energy. On the other hand, at bombarding energies of 2.4 and 2.7 GeV the primary reaction channel dominates such that we come closer to the results from the Glauber calculation. Furthermore, the difference between the parameter α obtained from the transport calculations to that from the Glauber model at beam energies $T_p=2.4$ and 2.7 GeV actually indicates the contribution from the secondary reaction mechanism.

The mass dependence of the ω production cross section including the FSI as resulting from the transport calculations is shown in Fig. 9 in comparison to the Glauber model employing a constant ωN cross section of 35 mb in the latter (dashed lines). The respective power law parameters α from the transport calculation differ with bombarding energy and approach $\alpha=2/3$ above $\simeq 2.4$ GeV bombarding energy characterizing the surface dominance of ω meson production in $p+A$ reactions due to strong absorption. On the other hand, the Glauber model gives a rough description of the mass dependence at higher energies for $\sigma_{\omega N}=35$ mb (with $\alpha \approx 0.55$). This sensitivity thus might also be explored experimentally, however, keeping in mind that the measurements should be performed at different bombarding energies to avoid systematic errors associated with different reaction mechanisms.

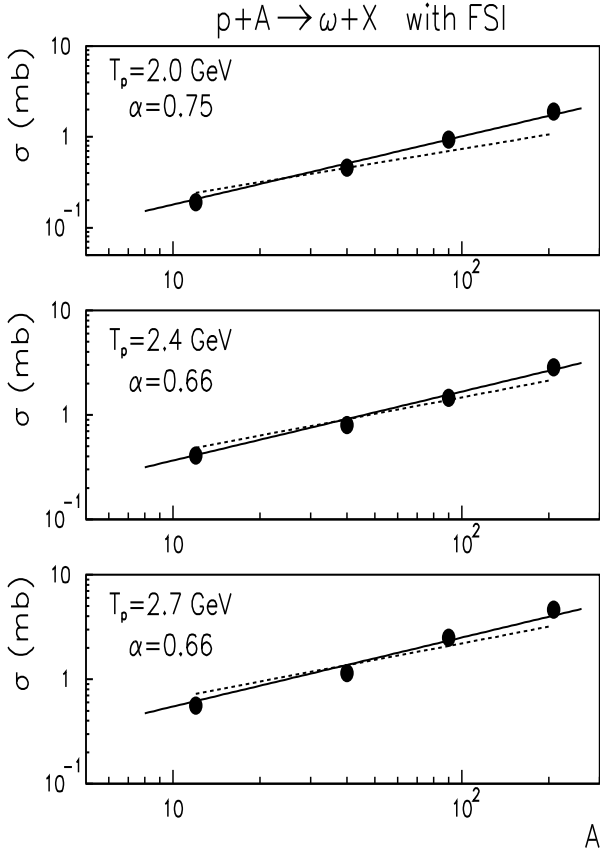


Fig. 9. The A -dependence of ω -meson production from $p+A$ reactions at beam energy $T_p=2.0, 2.4,$ and 2.7 GeV calculated with ωN FSI. The full dots show the transport model results while the solid lines are a fit by Eq. (13) with parameters α as indicated in the figures. The dashed lines show the calculations by the Glauber model for $\sigma_{\omega N}=35$ mb, which give $\alpha \approx 0.55$.

4 Summary

In this work we have explored the possibility to measure the elastic ωN cross section in $p+d \rightarrow d+\omega+p_{sp}$ reactions and the inelastic ωN cross section in $p+A$ collisions. Our studies based on MSMC and transport calculations indicate that the elastic scattering cross sections can be determined for ω momenta above 1 GeV/c in $p+d$ reactions by gating on high proton spectator momenta whereas the ωN absorption cross section is most effectively studied in $p+A$ reactions around $T_{lab}=2.4$ GeV via the mass dependence of the total production cross section. Though the apparent power law in the target mass A is sensitive to the actual strength of the ωN inelastic cross section, its actual momentum dependence cannot be extracted easily from experimental data due to strong effects from elastic ωN scattering processes.

Acknowledgments

We are grateful to G. Lykasov and M. V. Rzjanin for helpful discussions and access to their calculations prior to publication.

This work was supported in part by INTAS grant No. 96-0597, DFG, RFFI and Forschungszentrum Jülich.

References

1. W. Cassing and E. L. Bratkovskaya, Phys. Rep. **308**, (1999) 65.
2. R. Rapp and J. Wambach, hep-ph/9907502, to be publ. in Adv. Nucl. Phys.
3. W. Schön, A. Bokemeyer, W. König and V. Metag, Acta Physica Polon. B **27**, (1996) 2959.
4. W. Cassing, Ye. S. Golubeva, A. S. Iljinov and L. A. Kondratyuk, Phys. Lett. B **396**, (1997) 26.
5. Ye. S. Golubeva, L. A. Kondratyuk and W. Cassing, Nucl. Phys. A **625**, (1997) 832.
6. Th. Weidmann, E. L. Bratkovskaya, W. Cassing and U. Mosel, Phys. Rev. C **59**, (1999) 919.
7. G. E. Brown and M. Rho, Phys. Rev. Lett. **66**, (1991) 2720.
8. R. Rapp, G. Chanfray and J. Wambach, Nucl. Phys. A **617**, (1997) 472.
9. L. A. Kondratyuk, A. Sibirtsev, W. Cassing, Ye. S. Golubeva and M. Effenberger, Phys. Rev. C **58**, (1997) 1078.
10. F. Klingl and W. Weise, Nucl. Phys. A **606**, (1996) 329.
11. F. Klingl, N. Kaiser and W. Weise, Nucl. Phys. A **617**, (1997) 449.
12. F. Klingl, N. Kaiser and W. Weise, Nucl. Phys. A **624**, (1997) 927.
13. W. Peters, M. Post, H. Lenske, S. Leupold and U. Mosel, Nucl. Phys. A **632**, (1998) 109.
14. W. S. Chung, G. Q. Li and C. M. Ko, Nucl. Phys. A **625**, (1997) 325.
15. B. Friman, Acta Phys. Polon. B **29**, (1998) 3195.
16. G. I. Lykasov, W. Cassing, A. Sibirtsev and M. V. Rzjanin, Eur. Phys. Jour. A **6**, (1999) 71.
17. V. Yu. Grishina, L.A. Kondratyuk and M. Büscher, nucl-th/9906064
18. L.A. Kondratyuk, Sov. J. Nucl. Phys. **24**, (1976) 247.
19. L.A. Kondratyuk and M.Zh. Shmatikov, Phys. Lett. B **117**, (1982) 381.
20. A. Bianconi, S. Jeschonek, N.N. Nikolaev and B.G. Zakharov, Phys. Lett. B **343**, (1995) 13.
21. V.M. Kolybasov et al., Phys. Lett. B **222**, (1989) 135.
22. Ye.S. Golubeva, A.S. Iljinov, B.Krippa and I.A. Pshenichnov, Nucl. Phys. A **537**, (1992) 393.
23. Ye.S. Golubeva, A.S. Iljinov and I.A. Pshenichnov, Nucl.Phys. A **562**, (1993) 389.
24. R. Bizzarri et al., Nuovo Cimento A **22**, (1974) 225.
25. S.Ahmad et al., *Physics at LEAR with low-energy antiprotons* (eds. Amsler et al., Harwood Academic, New York 1987) 447.
26. M. Lacombe et al., Phys. Lett. B **101**, (1981) 139.
27. H. Calen et al., Phys. Rev. Lett. **79**, (1997) 2642.
28. H. Calen et al., Phys. Rev. Lett. **80**, (1998) 2069.
29. A. Sibirtsev and W. Cassing, Nucl. Phys. A **629**, (1998) 717.
30. W. Ehehalt and W. Cassing, Nucl. Phys. A **602**, (1996) 449.
31. Landolt-Börnstein, *New Series* (ed. H. Schopper, I/12 1988).
32. R.J. Glauber and J. Mathiae, Nucl. Phys. B **21**, (1970) 135.
33. B. Margolis, Phys. Lett. B **26**, (1968) 524.
34. B. Margolis, Nucl. Phys. B **4**, (1968) 433.
35. E. Vercellin et al., Nuovo Cim. A **106**, (1993) 861.
36. A. Sibirtsev, W. Cassing and U. Mosel, Z. Phys. A **358**, (1997) 357.
37. W. Cassing, *Proceedings of the WE-Heraeus-Seminar 'Hadronic Processes at Small Angles in Storage Rings'*, (ed. by E. Rössle and O.W.B. Schult) p. 167.
38. W. Cassing et al., Phys. Lett. B **238**, (1990) 25.
39. A. Sibirtsev and M. Büscher, Z. Phys. A **347**, (1994) 191.